ADVANCED ENERGY MATERIALS
www.advenergymat.de

Superionic Conduction of Sodium and Lithium in Anion-Mixed Hydroborates $Na_3BH_4B_{12}H_{12}$ and $(Li_{0.7}Na_{0.3})_3BH_4B_{12}H_{12}$

*Yolanda Sadikin, Matteo Brighi, Pascal Schouwink, and Radovan Černý**

It has been recognized that battery grids are one of the more realistic contenders for future large-scale energy storage.[1] A paradigm shift is taking place in battery research that is focusing on inexpensive and abundant chemical species as alternative to compensate for the dwindling resources of lithium in terms of charge carrier (electrolyte)[2] as well as a search for, in particular, Fe- and Mn-based electrode materials to replace current high-capacity electrodes based on costly transition metals such as Co or Ni.[3] These combined efforts target large-scale implementation, where low power density can be compensated for by quantity, and hence Na-based materials become one of the principal contenders. Many of the recent approaches employ a standard organic electrolyte, which imposes restrictions on the operating voltage window and the safety, for instance. This communication deals with the issue of the electrolyte. Superionic (solid-state) electrolytes contribute positively both to the working potential window as well as to safety aspects regarding the breakdown of the cell/grid.[4] Many such potential solid-state materials can be rationally designed from lithium or sodium salts containing dynamically disordered complex anions. The structure typically contains polyanions $[AB_y]^{n-}$ with covalent A—B bonds (e.g., PO_4^{3-}, SO_4^{2-} and NO_2^-), where the rotational diffusion of $[AB_y]^{n-}$ promotes cationic conductivity, decreasing the associated activation energy via the so-called "paddle-wheel" mechanism.[5] After the first reports on superionic metal borohydrides[6,7] based on the complex anion $[BH_4]^-$ and possible "paddle-wheel" mechanism in these compounds,[8] this concept was extended to higher boranes such as $[B_{10}H_{10}]^{2-}$ or $[B_{12}H_{12}]^{2-}$ in Na-based compounds.[9] It was shown by solid-state NMR and quasi-elastic neutron scattering[10] that the high rotational mobility promotes superionicity in the respective materials, whose conductivity increases by several orders of magnitude upon polymorphic order–disorder transformations into the superionic high-temperature (HT) phases, ≈0.1 S cm^{-1} (above 480 K) and 0.01 S cm^{-1} (above 380 K), respectively; however, transforming reversibly to the nonconducting phase upon temperature decrease. Currently, therefore, efforts are being invested to stabilize superionic conduction in such materials at room temperature (RT).

We have previously reported stable Cs- and Rb-borohydrides containing the *closo*-borane anion $[B_{12}H_{12}]^{2-}$ on the *A*-site of an inversed perovskite structure,[11] whose RT polymorph had already been reported for Cs[12] and forming during the decomposition of bi- and trimetallic borohydrides.[11] We suspected that the incorporation of both complex anions in the same structure could provide means of stabilizing compounds with high symmetry, favoring cationic mobility at RT. Herein, we apply this concept to anion-mixed metal boranes containing mobile species of relevance and present a novel class of solid electrolytes with the compounds $Na_3BH_4B_{12}H_{12}$ and $(Li_{0.7}Na_{0.3})_3BH_4B_{12}H_{12}$, capable of conducting either Na^+ or both Na^+ and Li^+ ions. Unlike order–disorder-governed dodeca- and decaboranes the cationic mobility is not entropically activated in $Na_3BH_4B_{12}H_{12}$ and $(Li_{0.7}Na_{0.3})_3BH_4B_{12}H_{12}$, thus requiring no HT phase transition. The conduction pathways in $Na_3BH_4B_{12}H_{12}$ are 2D where $Na_2B_{12}H_{12}$-like slabs are in fact nonconducting, reaching RT conductivity values close to the order of 10^{-3} S cm^{-1} and hence superior to many sulfide glasses, NASICON and rivaling even β-alumina.[13,14] $(Li_{0.7}Na_{0.3})_3BH_4B_{12}H_{12}$, on the other hand, forms 1D channels for mixed cation conduction. The chemical reaction forming the compound at 500 K is accompanied by a dramatic increase in ionic conductivity attaining values higher than 10^{-1} S cm^{-1} in the thermal stability region. Conductivity decreases upon cooling owed to full reversibility of the reaction. Such temperatures are nevertheless within reasonable limits for large-scale facilities, which operate at over 573 K in the case of Na–S power grids, for instance.

The new crystalline compounds $Na_3BH_4B_{12}H_{12}$ and $(Li_{0.7}Na_{0.3})_3BH_4B_{12}H_{12}$ form during thermal treatment of ball-milled mixtures composed of different combinations of $LiBH_4$, $NaBH_4$, $Li_2B_{12}H_{12}$, and $Na_2B_{12}H_{12}$. The in situ temperature-dependent diffraction data showing the phase formation are available in the Supporting Information (Figure S1). Ball milling is also attracting attention in battery research due to its flexibility and the ease with which it is brought to the industrial scale. It has recently been used to prepare promising Na-based materials.[13,15] We also recently employed it to scan a wide variety of perovskite-type metal–borohydride systems.[12,16] Here it is used to "activate" the powders, whereby no reaction takes place even at high energies. $(Li_{0.7}Na_{0.3})_3BH_4B_{12}H_{12}$ forms at 498 K (reaction onset) and dissociates to the precursors upon cooling. Meanwhile, the Na-rich $Na_3BH_4B_{12}H_{12}$ forms above 638 K, and once formed it maintains the same structure in a wide temperature range of 100–653 K. Differential scanning calorimetry was used to follow the thermal events for the evolution of $Na_3BH_4B_{12}H_{12}$

Y. Sadikin, M. Brighi, Dr. P. Schouwink, Prof. R. Černý
Department of Quantum Matter Physics
Laboratory of Crystallography
University of Geneva
Quai Ernest-Ansermet 24
1211 Geneva, Switzerland
E-mail: radovan.cerny@unige.ch

DOI: 10.1002/aenm.201501016

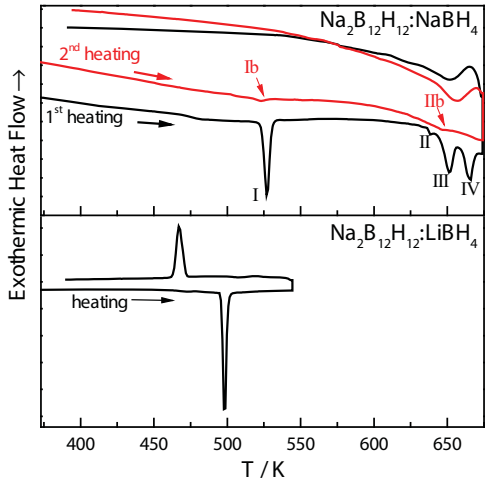

Figure 1. DSC measurement of the as-milled samples in sealed crucibles with heating/cooling rate 5 K min^{-1}: top) $Na_2B_{12}H_{12}$:$NaBH_4$ showing the phase formation and stabilization of compound $Na_3BH_4B_{12}H_{12}$ during first and second heating cycle and bottom) $Na_2B_{12}H_{12}$:$LiBH_4$ showing the formation and dissociation of $(Li_{0.7}Na_{0.3})_3BH_4B_{12}H_{12}$.

and is shown in **Figure 1** (top). Experiments were conducted in a sealed pan filled with 1 bar of argon to prevent mass loss since we assume the partial gas pressure to play a crucial role in stabilizing the compounds. At temperatures above 525 K, in the first heating cycle prior to formation of $Na_3BH_4B_{12}H_{12}$, the monoclinic-cubic phase transition of $Na_2B_{12}H_{12}$ is observed as an endothermic event (**I**), in agreement with the reported order–disorder transition.[17] Reaction (1) peaks at 638 K (**III**) and involves the melting of $NaBH_4$ at 673 K (event **II** could not be assigned), labeled as event **IV** in Figure 1. In situ diffraction data (Figure S1, Supporting Information) coincide with this event showing the vanishing of Bragg signals from the precursors and those emerging of the superionic phase. The formation of $Na_3BH_4B_{12}H_{12}$ proceeds via a solid-solid reaction on the surface $Na_2B_{12}H_{12}$ grains according to.

$$NaBH_{4(s)} + bcc\text{-}Na_2B_{12}H_{12(s)} \xrightarrow{638\,K} Na_3BH_4B_{12}H_{12(s)} \quad (1)$$

This results in an epitaxial relationship found in the crystal structures which are discussed below. Reaction (1) is completed at 673 K. We point out that $Na_3BH_4B_{12}H_{12}$ starts to dissociate again to its precursors if heated above 700 K, releasing molten $NaBH_4$ and solid bcc-$Na_2B_{12}H_{12}$ (Figure S2, Supporting Information). A peritectic point is thus predicted in the phase diagram $Na_2B_{12}H_{12}$:$NaBH_4$, with incongruent melting of the line phase $Na_3BH_4B_{12}H_{12}$, visible as event **IIb** in the second heating cycle. Upon cooling the melt below the liquidus it recrystallizes again. At the same time, if quenched within its thermal stability interval ($T < 700$ K), $Na_3BH_4B_{12}H_{12}$ remains stable during cooling to RT, also during the second heating/cooling cycle to 523 K, as shown in Figure 1 (the compound's stability is higher than 4 months in an Ar-filled glovebox). The coherent domain size in $Na_3BH_4B_{12}H_{12}$ was refined during cooling revealing a discrete step at the cubic-monoclinic phase transition temperature of $Na_2B_{12}H_{12}$ accompanied by a stepwise decrease of the unit cell volume (Figure S3, Supporting Information). We interpret this increase of the line broadening as fracturing of intergrown $Na_3BH_4B_{12}H_{12}$ grains. These results suggest that $Na_3BH_4B_{12}H_{12}$ is actually the stable phase at RT, and the as-milled composite is metastable.

The two-step formation of mixed-metal $(Li_{0.7}Na_{0.3})_2B_{12}H_{12}$ is described schematically as

$$LiBH_4 + Na_2B_{12}H_{12} \xrightarrow{\text{ball-milling}}$$
$$NaBH_4 + (Li_{1-x}Na_x)_2B_{12}H_{12} \underset{473\,K}{\overset{498\,K}{\rightleftharpoons}} (Li_{1-x}Na_x)_3BH_4B_{12}H_{12} \quad (2)$$

Ball-milling the precursors $Na_2B_{12}H_{12}$:$LiBH_4$ at high energies yields a composite of $NaBH_4$ and a mixed-metal *closo*-borane $(Li_{0.3}Na_{0.7})_2B_{12}H_{12}$. Reaction (2) proceeds at 498 K forming the compound $(Li_{0.7}Na_{0.3})_3BH_4B_{12}H_{12}$, visible as sharp endothermic peak in Figure 1 (bottom). The in situ diffraction data are available in the Supporting Information (Figure S1). Figure 1 (bottom) shows that reaction (2) is fully reversible, where during cooling $(Li_{0.7}Na_{0.3})_3BH_4B_{12}H_{12}$ segregates to the as-milled composite (Figure S1, Supporting Information).

A very similar reversible reaction is observed for the system $Li_2B_{12}H_{12}$:$NaBH_4$, which does not require a separate discussion in this communication. For the sake of completeness, we explored the system $Li_2B_{12}H_{12}$:$LiBH_4$ which, however, did not reveal similar phases. The mixture reacts at 543 K, producing a monoclinic phase whose crystal structure could presently not be solved.

The crystal structures of $Na_3BH_4B_{12}H_{12}$ and $(Li_{0.7}Na_{0.3})_3BH_4B_{12}H_{12}$ were solved ab initio with Fox[18] and are shown in **Figure 2**. Average positions are indicated for both Na and Li atoms. As it was not possible to locate cation positions unambiguously they were predicted as tetrahedral sites formed by anions, in agreement with the hitherto reported alkali metal-based *closo*-compounds.[19] Eight such sites were identified using TOPOS[20] and were then tested in Rietveld refinement with TOPAS,[21] constraining the total number of cations in the unit cell. These tetrahedra are formed by borohydrides and *closo*-anions either as 1+3 or 2+2. The only site formed exclusively by four *closos* was systematically refused by the refinement, leaving seven tetrahedral sites partly occupied in both compounds and giving rise to low-dimensional superionicity as discussed below.

The anion sublattice in turn is well characterized. Based on the anion positions only, we observe a distinct relationship between $Na_3BH_4B_{12}H_{12}$ and $(Li_{0.7}Na_{0.3})_3BH_4B_{12}H_{12}$, which is traced back to the simple relationship between the CrB[22] and FeB prototypes,[23] respectively. The space groups of both compounds are noncentrosymmetric subgroups of the prototypes: $Cmc2_1$ instead of $Cmcm$ for $Na_3BH_4B_{12}H_{12}$ (a = 8.0083(4), b = 21.881(1), c = 7.7672(4) Å, V = 1361.05(12) Å^3) at 523 K and $Pna2_1$ instead of $Pnam$ for $(Li_{0.7}Na_{0.3})_3BH_4B_{12}H_{12}$ (a = 14.9739(8), b = 11.5435(6), c = 7.5934(4) Å, V = 1312.5(1) Å^3) at 523 K. Inversion symmetry is lifted due to both the orientational order of anions and small shifts of the anions in the closoborane-borohydrides.

The *closo*-anion is ordered in both compounds, despite a mirror plane it is located on in $Na_3BH_4B_{12}H_{12}$. The BH_4 group occupies general position, seemingly ordered as well, though potential structural disorder of this anion cannot be deduced

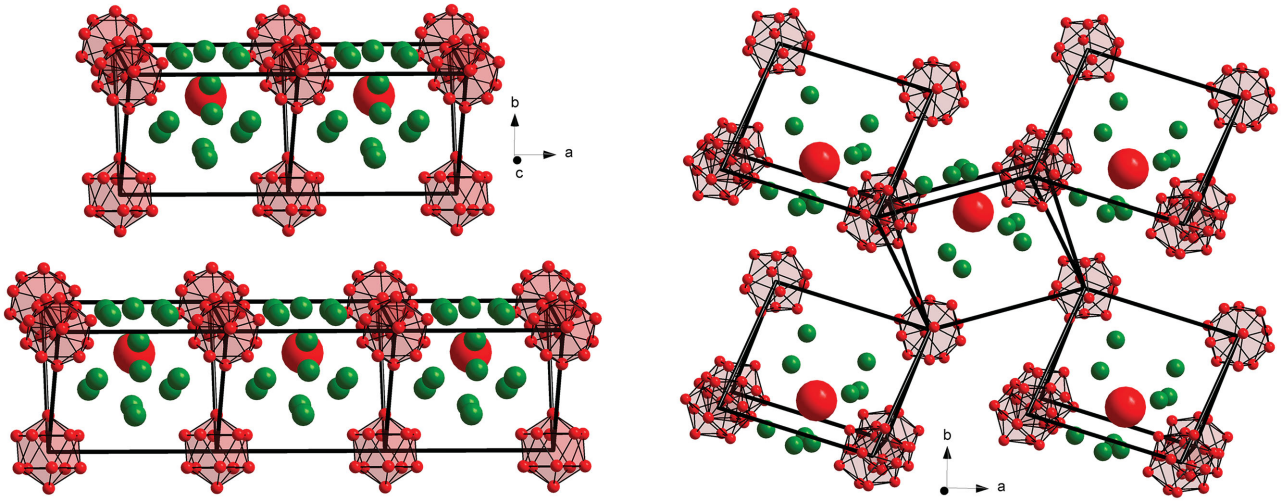

Figure 2. Crystal structure of mixed closoborane-borohydrides: left) *Cmc*2$_1$ $Na_3BH_4B_{12}H_{12}$ refined from data at 523 K and right) *Pna*2$_1$ $(Li_{0.7}Na_{0.3})_3BH_4B_{12}H_{12}$ refined from data at 523 K showing the connectivity and stacking of basic building units, trigonal prisms of *closo*-boranes. Only B atoms (red) of the closoboranes are shown; the borohydrides are shown simplified as big red spheres and cations as green spheres.

from SR-XPD. Both prototypes can be derived by twinning operations from *hcp* (FeB) or *ccp* (CrB) stacking of the larger atoms,[24] i.e., *closo*-boranes. Filling the interstitial sites of CrB-type $Na_3BH_4B_{12}H_{12}$ with the smaller Li cation stabilizes the FeB type. Given that FeB type and CrB type are two end members, there exist several stacking variants between them,[25] which could possibly form along the hypothetical binary phase diagram $Na_3BH_4B_{12}H_{12}$–$Li_3BH_4B_{12}H_{12}$, hence providing a roadmap for future studies on mixed-borane superionics. The Rietveld plots and structural parameters of the discussed structures are available as Figures S4–S6 (Supporting Information) and deposited CIF files.

The *T*-dependence of the ionic conductivity σ was investigated with electrochemical impedance spectroscopy. **Figure 3** (inset) shows the Nyquist plots obtained for $Na_3BH_4B_{12}H_{12}$ using a pair of gold (Au) discs as ion-blocking electrodes and sodium (Na) foil as nonblocking electrodes. A semicircle with a spike in the low-frequency regime evidences blocking of Na-ions by the electrode in the Au cell. Using Na foils the electrode contribution (spike) is removed and $Na_3BH_4B_{12}H_{12}$ shows only a semicircle, from which σ is determined.

The temperature dependency of σ is shown in Figure 3. All as-milled mixtures, which contain only composites of borohydride and *closo*-borane phases, show higher values for the conductivity at RT relative to the as-received $Na_2B_{12}H_{12}$. This effect is associated with mechanochemical processing and the grain morphology of the powder. Upon temperature increase, a remarkable increase is observed in the conductivity of all composite mixtures which is assigned to the chemical reactions forming the mixed closoborane-borohydride phases. The reversibility of the chemical reaction $Na_2B_{12}H_{12}$:$LiBH_4$ forming $(Li_{0.7}Na_{0.3})_3BH_4B_{12}H_{12}$ results in a conductivity decrease upon cooling with a hysteresis of 17 K, which correlates well with the phase composition determined from in situ diffraction data (Figure S1, Supporting Information). $Na_3BH_4B_{12}H_{12}$, on the other hand, is stable to RT once synthesized and its RT Na conductivity is approximately at 0.5×10^{-3} S cm^{-1}, which is more than two orders of magnitude higher than the only other Na-conducting borohydride material $Na_2BH_4NH_2$ (at 2×10^{-6} S cm^{-1})[26] and comparable to the most promising Na-based superionic currently under evaluation, such as β-alumina,[27] NASICON,[14] or sulfide-based glass ceramics.[13] This presents hence the best conducting BH_4 material. The activation energies $E_a(Na^+)$ for the hops between different accessible sites were determined from the Arrhenius plots where two linear regions of different slopes are fitted, the obtained values amounting to 340 meV (273–468 K) and 517 meV (218–273 K). The Na ion is therefore highly mobile over a wide temperature range. Regarding the reported superionic *closo*-materials the Na conduction in $Na_3BH_4B_{12}H_{12}$ is facilitated with respect to $Na_2B_{10}H_{10}$ (470 meV) and below that of $Na_2B_{12}H_{12}$ (210 meV).[8]

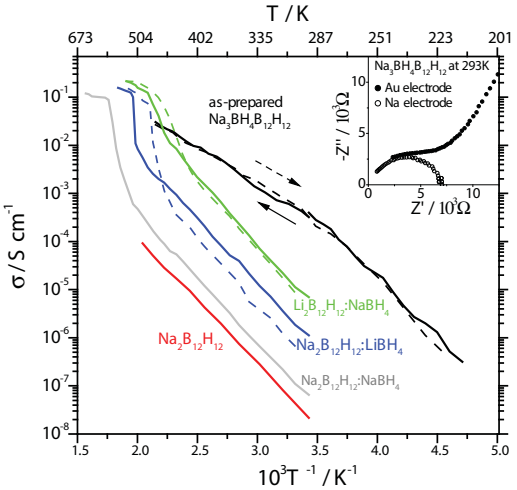

Figure 3. Temperature dependence of the AC conductivity of as-milled samples $M_2B_{12}H_{12}$:MBH_4 (M = Li, Na) and as-prepared $Na_3BH_4B_{12}H_{12}$. Conductivity of starting material $Na_2B_{12}H_{12}$ is shown for comparison. Inset: Nyquist plots of $Na_3BH_4B_{12}H_{12}$ using a pair of Au or Na electrodes measured at 293 K (pellet thickness 1.5 mm).

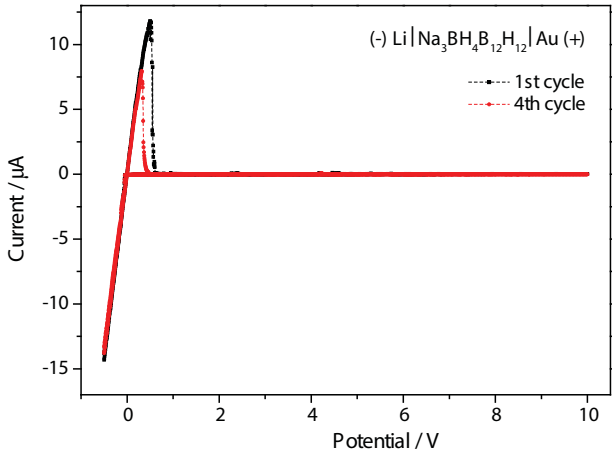

Figure 4. Cyclic voltammogram of $Na_3BH_4B_{12}H_{12}$ measured at 293 K (scan rate 50 mV s^{-1}, pellet thickness 1 mm).

In contrast to $Na_3BH_4B_{12}H_{12}$, the latter do not exhibit superionic conduction at RT. Mixed-anion borohydride amide materials such as $Li_2(BH_4)(NH_2)$ (560 meV), $Li_4(BH_4)(NH_2)_3$ (260 meV), or $Na_2BH_4NH_2$ (610 meV) show comparable activation energies even at RT, however with lower cationic conductivity of 2×10^{-4} and 2×10^{-6} S cm^{-1}.[26,28] $LiBH_4$ itself again has both a higher activation energy (560 meV) and higher transition temperature of the superionic phase.[6]

We so far have no explanation for the discontinuity in $E_a(Na^+)$ at 273 K in as-prepared $Na_3BH_4B_{12}H_{12}$. The sample is stable in the AC cell and diffraction shows a pure phase sample after various cycles in the respective temperature range. The gradual thermal activation of disorder of the BH_4 group may be at the origin of this, which has previously been observed in metal borohydrides,[29] and will require future investigations on the structural dynamics by means of NMR or QENS.

The thermal stability field of $(Li_{0.7}Na_{0.3})_3BH_4B_{12}H_{12}$ is very restricted within the investigated temperature range (Figure 3) and it was not possible to determine reliable activation energies. At temperatures above the chemical reaction forming the phase the conductivity reaches values beyond 10^{-1} S cm^{-1}.

The electrochemical window of $Na_3BH_4B_{12}H_{12}$ shown in **Figure 4** was determined at RT with cyclic voltammetry using an asymmetric setup with Na and Au electrodes. Cathodic and anodic currents respectively were observed near 0 V showing reversible sodium plating ($Na^+ + e^- \rightarrow Na$) and stripping ($Na \rightarrow Na^+ + e^-$). The absence of any further current up to 10 V versus Na/Na^+ allows us to exclude electrochemical reactions and confirm the electrochemical stability of $Na_3BH_4B_{12}H_{12}$. Such a wide potential window suggests the material to be a suitable electrolyte for high-power batteries utilizing cathodes with very high positive voltages versus Na/Na^+.

To determine the volume accessible to mobile species, a structural analysis was carried out with TOPOS[20] on both mixed-anion compounds. The anion submatrix, from which the voids are extracted, was built from boron atomic positions only.

The conduction pathways are shown in **Figure 5**. It is striking that there is a dimensionality change in superionic behavior between both compounds despite the identical anion stoichiometry. The refined average positions of mobile Na in $Na_3BH_4B_{12}H_{12}$ come to lie in structural fragments containing the BH_4 anion (Figure 2), which can be rationalized as layers perpendicular to the *b*-axis, in analogy to CrB. Thus, regions of high Na density alternate with Na-free slabs built from the *closo*-anion. The layered character of the compound is also reflected in the temperature dependency of the lattice parameters as revealing lower thermal expansion for the *b*-axis while that of *a* and *c* is very similar (Figure S7, Supporting Information). The conduction pathways show that Na-free regions are not interconnected with Na-rich slabs, manifesting a 2D mechanism occurring in mixed-anion slabs. Though this is not expected, given the high conductivity of $Na_2B_{12}H_{12}$, we remind that the *closo*-anions in these structures are not crystallographically disordered (though they may be on a different time scale). In superionic HT-$Na_2B_{12}H_{12}$ Na atoms hop between interstitial tetrahedral sites via the longest edges of the *closo*-tetrahedron, with a length of 8.098 Å, the shorter edges (7.013 Å) are energetically unfavored. Nonconducting LT-$Na_2B_{12}H_{12}$ has maximum edge lengths of 7.422 Å. In $Na_3BH_4B_{12}H_{12}$, the nonconducting slabs form sheets of edge-sharing tetrahedra with an intrasheet edge length of 7.139 Å. The edges connecting to the mixed-anion slabs are considerably longer, reaching 8.008 Å. Hence, while Na ions may enter the *closo*-slab, the higher energy barrier for conduction within the slab presents the bottleneck of the conduction path and favors superionicity in the mixed-anion slab.

Interestingly, the conduction pathways are topologically different in mixed-cation $(Li_{0.7}Na_{0.3})_3BH_4B_{12}H_{12}$, for the Li^+ ion (3D) and the Na^+ ion (1D). It is best seen from Figure 2 that Na mobility is again associated with structural fragments

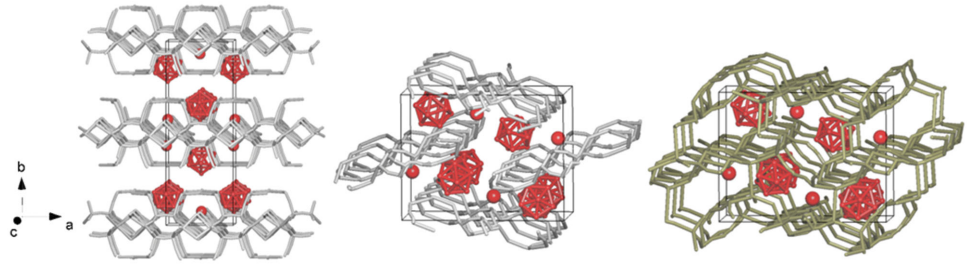

Figure 5. Left) Anion framework and continuous 2D migration path (010) for Na ion constructed from possible voids and channels in the structure of $Na_3BH_4B_{12}H_{12}$. Centre and right) For mixed cation conductors $(Li_{0.7}Na_{0.3})_3BH_4B_{12}H_{12}$, the anion framework can provide continuous 1D migration path [001] for Na ion (gray channels) and 3D migration path for Li ion (yellow channels). All refined positions of cations coincide with the calculated voids.

containing mixed anions, while the *closo*-areas are not included. This leads to 1D conduction channels for Na. On the other hand, sufficient voids and channels are accessible to the smaller Li^+ ion, in order to allow for 3D superionic behavior.

As a means of altering the physical properties of borohydrides the substitution $BH_4^- \leftrightarrow$ halide has often been employed to manipulate, e.g., hydrogen release, structural behavior, phase stabilities, or ionic conductivity.[30] Referring to this new family of mixed-anion boranes discussed herein, we have attempted to apply this concept to $Na_3BH_4B_{12}H_{12}$, which we consider as the model compound from now on.

Anion substitution $BH_4^- \leftrightarrow I^-$ in $Na_3BH_4B_{12}H_{12}$ was investigated by reacting NaI with $Na_2B_{12}H_{12}$, in order to obtain a compound free of BH_4 and thus less prone to hydrolyze. The substitution for iodide is known to occur easily and has been reported various times. As observed for many mixed-metal mixtures based on *closo*-precursors no reaction takes place during milling. The mixture was reacted by heating the as-milled mixture to 923 K and monitored by in situ diffraction. The resulting product contains a single main phase which was solved ab initio as an antiperovskite-derived compound $Na_3IB_{12}H_{12}$ (Rietveld plot and structural model as Figure S8 in the Supporting Information) with two half occupied Na positions, indicating significant cationic disorder. We hence expect this phase to have a high Na mobility. Interestingly, the replacement of tetrahedral BH_4^- by spherical I^- leads to a different structure type. The antiperovskite and CrB type are, however, related by a crystallographic shear.[24] Currently, we have not succeeded in producing a sufficient sample amount to study its ionic conductivity, information on its superionic behavior is thus not yet available, but ongoing efforts are focusing on this, since antiperovskite systems with a CsCl-type arrangement of anions, such as $XONa_3$ (X = NO_2, Br, CN)[5] and $XOLi_3$ (X = Cl, Br)[31] have been demonstrated to favor superionic conductivity.

In summary, the first metal closoborane-borohydrides have shown to favor ionic conductivity of both Li and Na cations. For the first time, a borohydride-based material reaches RT conductivity values of close to 10^{-3} S cm^{-1}. The high electrochemical stability and rather low activation energy of down to 340 meV reveal potential of the materials to work well in high voltage applications. Investigations on the structural dynamics at various timescales are required next to gain detailed insight into the conduction mechanism and the extent to which structural dynamics are actually involved, which play the dominant role in the superionic phases of Na closoboranes but have herein been found to of lesser importance in closoborane-borohydrides; an important finding since it does not require thermal activation of ionic motion and RT superionics can thus be realized.

In structural analogy to the FeB and CrB types, the $(Li_{1-x}Na_x)_3BH_4B_{12}H_{12}$ family is expected to contain further stacking variants in the MBH_4–$M_2B_{12}H_{12}$ (M = Li, Na) phase diagram, which could exhibit superionic conduction and be used as double-cation solid-state electrolytes in mixed Li^+/Na^+ batteries.[32] Next to this, mixed-anion compounds based on other complex anions such as $[B_{10}H_{10}]^{2-}$ will be explored in the future in a search for tailor-made crystalline solids with improved performance as solid-state electrolytes.

Experimental Section

Synthesis: LiBH4 (>95%), NaI (99%), and NaBH4 (96%) were purchased from Sigma-Aldrich, $Na_2B_{12}H_{12}$ (98.5%) from Katchem. $Li_2B_{12}H_{12}$ was prepared according to reference.[33] The reactants were mixed in 1:1 $M_2B_{12}H_{12}$:MBH_4 or NaI ratio (M = Li, Na), and milled at 400 rpm in a Fritsch Pulverisette 7 premium line at 30 2 min with 2 min breaks. The powder-to-ball mass ratio was 1:50. $Na_3BH_4B_{12}H_{12}$ was prepared by mechanical milling and consecutive heat treatment to 673 K in aluminum crucibles in a closed system at rate of 5 K min^{-1}. The cation-mixed compound $(Li_{0.7}Na_{0.3})_3BH_4B_{12}H_{12}$ was prepared by ball milling 1:1 mixtures of $Na_2B_{12}H_{12}$ and $LiBH_4$ and heating the sample to 493 K in a closed system. It can also be prepared by ball milling a 1:1 mixture of $Li_2B_{12}H_{12}$ and $NaBH_4$ and a heating to 463 K in a closed system. It cannot be quenched to RT. All sample handling was done in a glovebox under argon atmosphere.

Synchrotron Radiation X-Ray Powder Diffraction (SR-XPD): The data used for crystal structure solution and refinements were collected between 298 K and 823 K at the Swiss–Norwegian Beamlines of ESRF (European Synchrotron Radiation Facility, Grenoble, France). Data were recorded on a Dectris Pilatus M2 detector at a wavelength of 0.68884 and 0.81701 Å calibrated with an NIST SRM660b LaB_6 standard. The temperature was controlled with a hot air blower; 2D images were integrated and treated with FIT2D.[34] Another data set has been collected at the Materials Science beamline at the SLS (Villigen, Switzerland). Data were recorded with 1D silicon strip detector Mythen-II at a wavelength of 0.77487 Å calibrated with an NIST SRM660b LaB_6 standard. The temperature was controlled with a hot air blower. All samples were measured in borosilicate capillaries (0.5 mm) spun during data acquisition. Details on structure solution and refinement are presented in the Supporting Information.

Differential Scanning Calorimetry (DSC): Measurements were carried out on a Netzsch STA449 F3 Jupiter from 298 K to 673 K at a ramping rate of 5 K min^{-1} using sealed Al crucibles as sample holder. Approximately 2.5 mg of sample was used for each run.

AC and DC Conductivity: The powder was cold-pressed into a pellet (diameter 3.175 mm, thickness ≈0.8–1.5 mm corresponds to 85%–90% of the theoretical density) and spring loaded between Au or Na electrodes inside a Novocontrol sample cell BDS 1200. Electrochemical impedance spectroscopy (EIS) was performed using an HP4192A LF impedance analyzer (frequency range 1 kHz–2 MHz, applied voltage 10 mV). Bulk conductivities were derived from interpreting circular arcs and/or spike intercept on the x-axis. Cyclic voltammetry was carried out by measuring the current–voltage response using a PC-controlled National Instrument PXI data acquisition.

Conduction Path Analysis: The possible cationic conduction paths of the refined structures were determined by using Voronoi-Dirichlet Polyhedra (VDP) analysis implemented in the program package TOPOS.

All hydrogens were removed for simplification purpose, $[B_{12}H_{12}]^{2-}$ group is represented by a B_{12} cage while $[BH_4]^-$ group is represented by a single B atom, so the voids and channels for cationic conduction are determined only by boron atoms. The channel was constructed by connecting voids that are large enough to accommodate a cation (radius of void sphere R_{sd} > 1.13 Å). A conduction path is said to exist if the channel is continuous in at least one direction and the radius of channel is close to cation–anion distance (R_{ca}), with R_{ca}(Li–B) > 2.62 Å and R_{ca}(Na–B) > 2.66 Å.

Supporting Information

Supporting Information is available from the Wiley Online Library or from the author. Further details of the crystal structure investigations may be obtained from the Fachinformationszentrum Karlsruhe, 76344 Eggenstein-Leopoldshafen (Germany), on quoting the depository numbers CSD-429705 and CSD-429706.

Acknowledgements

This work was supported by the Swiss National Science Foundation. The authors acknowledge the Swiss-Norwegian Beamlines of ESRF and the Materials Science beamline of the SLS for the allocation of beamtime and excellent support with the data collection. The authors thank Prof. Hai-Wen Li for providing $Li_2B_{12}H_{12}$ for the synthesis. The authors thank Prof. Hans Hagemann and Manish Sharma for access and support for DSC/TG equipment.

Received: May 22, 2015
Revised: July 2, 2015
Published online:

[1] a) V. Palomares, P. Serras, I. Villaluenga, K. B. Hueso, J. Carretero-Gonzalez, T. Rojo, *Energ Environ Sci.* **2012**, *5*, 5884; b) K. Kubota, N. Yabuuchi, H. Yoshida, M. Dahbi, S. Komaba, *Mrs Bull.* **2014**, *39*, 416; c) B. Dunn, H. Kamath, J. M. Tarascon, *Science* **2011**, *334*, 928.
[2] J. M. Tarascon, *Nat. Chem.* **2010**, *2*, 510.
[3] a) A. Yamada, *MRS Bull.* **2014**, *39*, 423; b) B. C. Melot, D. O. Scanlon, M. Reynaud, G. Rousse, J. N. Chotard, M. Henry, J. M. Tarascon, *Acs Appl Mater Inter.* **2014**, *6*, 10832; c) N. Yabuuchi, S. Komaba, *Sci. Technol. Adv. Mat.* **2014**, *15*, 043501.
[4] N. Yabuuchi, K. Kubota, M. Dahbi, S. Komaba, *Chem. Rev.* **2014**, *114*, 11636.
[5] M. Jansen, *Angew. Chem. Int. Ed.* **1991**, *30*, 1547.
[6] M. Matsuo, Y. Nakamori, S. Orimo, H. Maekawa, H. Takamura, *Appl. Phys. Lett.* **2007**, *91*, 224103.
[7] M. B. Ley, D. B. Ravnsbaek, Y. Filinchuk, Y. S. Lee, R. Janot, Y. W. Cho, J. Skibsted, T. R. Jensen, *Chem. Mater.* **2012**, *24*, 1654.
[8] a) P. Martelli, A. Remhof, A. Borgschulte, R. Ackermann, T. Strassle, J. P. Embs, M. Ernst, M. Matsuo, S. I. Orimo, A. Zuttel, *J. Phys. Chem. A.* **2011**, *115*, 5329; b) N. Verdal, T. J. Udovic, J. J. Rush, H. Wu, A. V. Skripov, *J. Phys. Chem. C.* **2013**, *117*, 12010; c) A. V. Skripov, A. V. Soloninin, M. B. Ley, T. R. Jensen, Y. Filinchuk, *J. Phys. Chem. C.* **2013**, *117*, 14965.
[9] a) T. J. Udovic, M. Matsuo, A. Unemoto, N. Verdal, V. Stavila, A. V. Skripov, J. J. Rush, H. Takamura, S. Orimo, *Chem. Commun.* **2014**, *50*, 3750; b) T. J. Udovic, M. Matsuo, W. S. Tang, H. Wu, V. Stavila, A. V. Soloninin, R. V. Skoryunov, O. A. Babanova, A. V. Skripov, J. J. Rush, A. Unemoto, H. Takamura, S. Orimo, *Adv. Mater.* **2014**, *26*, 7622.
[10] a) A. V. Skripov, O. A. Babanova, A. V. Soloninin, V. Stavila, N. Verdal, T. J. Udovic, J. J. Rush, *J. Phys. Chem. C.* **2013**, *117*, 25961; b) N. Verdal, T. J. Udovic, V. Stavila, W. S. Tang, J. J. Rush, A. V. Skripov, *J. Phys. Chem. C.* **2014**, *118*, 17483.
[11] Y. Sadikin, K. Stare, P. Schouwink, M. Brix Ley, T. R. Jensen, A. Meden, R. Černý, *J. Solid. State. Chem.* **2015**, *225*, 231.
[12] I. Tiritiris, *PhD Thesis*, Universität Stuttgart, Stuttgart **2004**.
[13] A. Hayashi, K. Noi, A. Sakuda, M. Tatsumisago, *Nat. Commun.* **2012**, *3*, 856.
[14] O. Bohnke, S. Ronchetti, D. Mazza, *Solid State Ionics* **1999**, *122*, 127.
[15] P. Barpanda, G. Oyama, S. Nishimura, S. C. Chung, A. Yamada, *Nat. Commun.* **2014**, *5*, 4358.
[16] P. Schouwink, M. B. Ley, A. Tissot, H. Hagemann, T. R. Jensen, L. Smrčok, R. Černý, *Nat. Commun.* **2014**, *5*, 5706.
[17] N. Verdal, J. H. Her, V. Stavila, A. V. Soloninin, O. A. Babanova, A. V. Skripov, T. J. Udovic, J. J. Rush, *J. Solid State Chem.* **2014**, *212*, 81.
[18] V. Favre-Nicolin, R. Černý, *J. Appl. Crystallogr.* **2002**, *35*, 734.
[19] N. Verdal, W. Zhou, V. Stavila, J. H. Her, M. Yousufuddin, T. Yildirim, T. J. Udovic, *J. Alloys Compd.* **2011**, *509*, S694.
[20] V. A. Blatov, *Struct. Chem.* **2012**, *23*, 955.
[21] A. A. Coelho, *J. Appl. Crystallogr.* **2000**, *33*, 899.
[22] L. Helmholz, *Z. Kristallogr.* **1936**, *95*, 129.
[23] T. Bjurström, *Ark. Kemi Mineral. Geol.* **1933**, *11A*, 1.
[24] B. G. Hyde, S. Andersson, *Inorganic Crystal Structures*, Wiley, New York **1989**.
[25] K. Klepp, E. Parthe, *Acta. Crystallogr. B.* **1981**, *37*, 495.
[26] M. Matsuo, S. Kuromoto, T. Sato, H. Oguchi, H. Takamura, S. Orimo, *Appl. Phys. Lett.* **2012**, *100*, 203904.
[27] A. Hooper, *J. Phys. D: Appl. Phys.* **1977**, *10*, 1487.
[28] M. Matsuo, A. Remhof, P. Martelli, R. Caputo, M. Ernst, Y. Miura, T. Sato, H. Oguchi, H. Maekawa, H. Takamura, A. Borgschulte, A. Zuttel, S. Orimo, *J. Am. Chem. Soc* **2009**, *131*, 16389.
[29] D. Blanchard, J. B. Maronsson, M. D. Riktor, J. Kheres, D. Sveinbjornsson, E. G. Bardaji, A. Leon, F. Juranyi, J. Wuttke, K. Lefmann, B. C. Hauback, M. Fichtner, T. Vegge, *J. Phys. Chem. C.* **2012**, *116*, 2013.
[30] A. Unemoto, M. Matsuo, S. Orimo, *Adv. Funct. Mater.* **2014**, *24*, 2267.
[31] Y. S. Zhao, L. L. Daemen, *J. Am. Chem. Soc.* **2012**, *134*, 15042.
[32] L. Chen, Q. W. Gu, X. F. Zhou, S. X. Lee, Y. G. Xia, Z. P. Liu, *Sci Rep-Uk.* **2013**, *3*, 1946.
[33] L. Q. He, H. W. Li, S. J. Hwang, E. Akiba, *J. Phys. Chem. C.* **2014**, *118*, 6084.
[34] A. P. Hammersley, S. O. Svensson, M. Hanfland, A. N. Fitch, D. Hausermann, *High Pressure Res.* **1996**, *14*, 235.